09

Method for extraction of frequency-dependent attenuation and coupling coefficients of optical microring resonator coupled with straight waveguide

© A.A. Nikitin, K.N. Chekmezov, A.A. Ershov, A.A. Semenov, A.B. Ustinov

St. Petersburg Electrotechnical University „LETI"
197022 St. Petersburg, Russia
email: aanikitin@etu.ru

Received March 4, 2024
Revised May 2, 2024
Accepted May 31, 2024

An original non-destructive characterization method of basic components of photonic integrated circuits in a wide frequency range is proposed. The method allows extracting a frequency-dependent coupling coefficient of the microring resonator with a straight waveguide, as well as the attenuation coefficient, group refractive index and dispersion coefficient of rectangular optical waveguide from the measured transmission characteristics of the microring resonator serving as a test element. An efficiency of the proposed characterization method is demonstrated for photonic integrated circuits fabricated by a silicon-on-insulator technology in the frequency range of 184–197 THz (which corresponds to the wavelength range of 1520–1630 nm). Obtained waveguide parameters are used for modeling the transmission characteristics of the photonic integrated circuits that are in good agreement with experimental data.

Keywords: photonic integrated circuits, optical waveguides, silicon-on-insulator, non-destructive characterization methods.

DOI: 10.61011/TP.2024.08.59017.72-24

Introduction

Currently, photonic integrated circuit (PIC) technologies for creating compact photonic and microwave photonic devices demonstrate an active development. Silicon nitride, silicon, indium phosphide, and thin-film lithium niobate are the most promising materials for PIC manufacturing [1,2]. „Silicon-on-insulator" (SOI) is one of the main technological platforms for creating integrated photonics devices [3]. This technology is compatible with CMOS (complementary metal-oxide-semiconductor structure) technology for manufacturing integrated circuits of microelectronics. In addition, the bending radius of silicon waveguides can be reduced to $5\,\mu$m owing to the high contrast of refractive indices with negligibly low radiation losses [4–6], which makes it possible to create PICs with a high element density [7–9].

Not only passive optical devices, such as filters, directional couplers, multiplexers and demultiplexers [10–15], but also modulators [16,17] can be manufactured on the basis of SOI technology, as well as silicon-germanium waveguide photodetectors [18,19]. In addition, the variety of nonlinear effects in silicon waveguides [20] allows creating various nonlinear devices, such as memory cells, logic gates, switches and transistors [21–24], which find their application for implementing artificial neural networks [25,26]. Silicon nitride is another promising material for creating passive integrated microwave photonics devices. The key advantage of this material is the record low propagation loss (less than dB/m), which is unattainable for silicon waveguides [27–29]. Therefore, one of the most relevant areas of development of PIC technology is the combination of SOI with silicon nitride technology (SiN-on-SOI) [9,30].

Methods for determining the waveguide parameters of manufactured optical waveguides are necessary for the development of new technological platforms, as well as for the mass production of PICs. The key waveguide parameters are the attenuation coefficient and propagation constant. In addition, PIC often uses coupled waveguide structures, so another important parameter is the coupling coefficient, for example, between a waveguide and a microring resonator (MRR). Fiber-optic communication lines are used to transmit optical signal between the PIC, so the spectral efficiency of input/output grating couplers should also be known. Therefore, an urgent task is to develop methods for determining the frequency dependences of the above parameters of silicon and silicon-nitride PICs.

Methods for studying optical waveguides can be divided into destructive and non-destructive. Destructive methods are usually aimed at direct measurement of the geometry of structures. Then the listed parameters of PIC waveguides can be obtained by numerical modeling for known material parameters. Such methods require partial or complete destruction of the coating layer or the entire chip. These methods include, for example, confocal, atomic force, or scanning electron microscopy [31]. The cut-back technique is another method for determining the waveguide properties of PICs [4,32,33]. This method measures the insertion loss of a device, for example, a ring resonator with a different

length of the input waveguide [34]. The slope of the resulting dependence of the insertion loss on the waveguide length determines attenuation coefficient. If the input waveguide length is zero, the attenuation is determined only by coupling losses, which can be extracted by extrapolating the obtained dependence.

In nondestructive methods the waveguiding properties are usually determined from the measured transfer characteristics of a test element. Various interference circuits can be used for the PIC characterization [6]. For example, the transfer characteristics of Fabry-Perot [34–38] or Mach-Zehnder [39] interferometers can be used to determine the propagation losses and dispersion properties of microwaveguides, as well as the geometry of the waveguide structures [31]. However, the coupling coefficients of the ring resonator with the straight microwaveguides could not be defined by such methods. Nevertheless these values are necessary for designing of PICs. It should be noted that the coupling and attenuation coefficients cannot be expressed explicitly using the experimental transfer characteristics of a ring resonator. A method based on the measurement of the transfer characteristics of a set of test elements, namely a direct microwaveguide, a waveguide coupler, a micro-ring resonator, and a Mach-Zehnder interferometer was proposed to independently determine these coefficients, as well as the dispersion properties of the PIC. The measurement of the transfer characteristics of such a set of test elements makes it possible to determine each of the waveguide parameters of the PIC separately [40]. The disadvantage of this approach is that it requires the use of several elements, the waveguide properties of which may vary due to inhomogeneities attributable to the manufacturing technology [8,31].

The backscattering reflectometry is another method for determining the propagation losses and MRR coupling coefficient. The parameters of the ring resonator are determined from reflectograms in this case [41–43]. This method makes it possible to extract both the attenuation and coupling coefficients and the dispersion properties of optical microwaveguides. It should be noted that this method is not applicable when performing measurements in a wide frequency range, especially in the case of a strong frequency dependence of the measured parameters.

A method was proposed in [44] in which the experimental values of the width and depth of the MRR resonance absorption line were determined from the experimental transfer characteristics of a ring resonator coupled to a single input waveguide. The obtained data were used to compile a system of two equations. The attenuation and coupling coefficients were obtained from the solution of this system. The functionality of such a method can be significantly enhanced by including the MRR in one of the arms of the Mach-Zehnder interferometer [45], which makes it possible to determine not only the coupling coefficients and losses, but also the attenuation in the coupling region [46]. However, the need to determine the width of the resonance curve limits the applicability of this method both in the case of high attenuation in waveguides and with the coupling coefficient close to the limit values [44].

A method is proposed in this paper in which the waveguide parameters are extracted from the experimental values of the minima and maxima of the transfer characteristics of a test micro-ring resonator symmetrically coupled with two input waveguides. The method allows local determination of the attenuation and coupling coefficients of the PICs in a broad frequency range.

1. Description of the studied structures and measurement methods

This paper studied MRR with diameters of $d = 20$, 100 and 256 μm made using commercial SOI technology. The scheme of measurement setup and topology of the studied MRR are shown in Fig. 1, *a*. The studied structures were formed from rectangular silicon microwaveguides with cross-section of 500×220 nm. The cross-section of waveguides is shown in Fig. 1, *b*. In addition, this figure shows the profile of the TE mode at a frequency of 193.4 THz (wavelength 1550 nm) obtained using the method of Finite Difference Time Domain (FDTD).

The width of the gap between the straight waveguide and the MRR is 200 nm. The transfer characteristics of the MRR were measured in the frequency range from 184 to 197 THz using High Definition Component Analyzer (HDCA) manufactured by Aragon Photonics. The analyzer has an internal tunable laser source that allows measurements for TE and TM polarization in the C and L optical bands. Measurements, the results of which will be presented below, were obtained for the case of TE-polarization.

Lensed fibers by OZ Photonics with antireflection coating, a focal spot size of 5 μm and a focal length of 26 μm were used for radiation input and output. The fibers were secured in linear translators. Diffraction gratings were used as coupling elements in the scheme. The radiation input/output angle was selected to ensure the highest input efficiency and, accordingly, the maximum transmission coefficient in the frequency range under investigation. A microscope with a digital camera was used for visual inspection. The studied resonators have several outputs, so when measuring the transfer characteristics, the receiving fiber moved between the outputs *2* and *3*, as shown by the arrow in Fig. 1, *a*. It should be noted that the power of the input signal P_{in} was selected during measurements in such a way as to ensure the linear operation of the studied micro-ring resonators. The input signal power during measurements of the transfer characteristics of a resonator with a diameter of $d = 256\,\mu$m was $P_{in} = 0$ dBm, for $d = 100\,\mu$m — $P_{in} = -10$ dBm and for $d = 20\,\mu$m — $P_{in} = -18$ dBm. The HDCA built-in optical attenuator was used to control the input signal power.

Measured transfer characteristics of MRRs with diameters of $d = 20$, 100 and 256 μm are shown in Figure 2

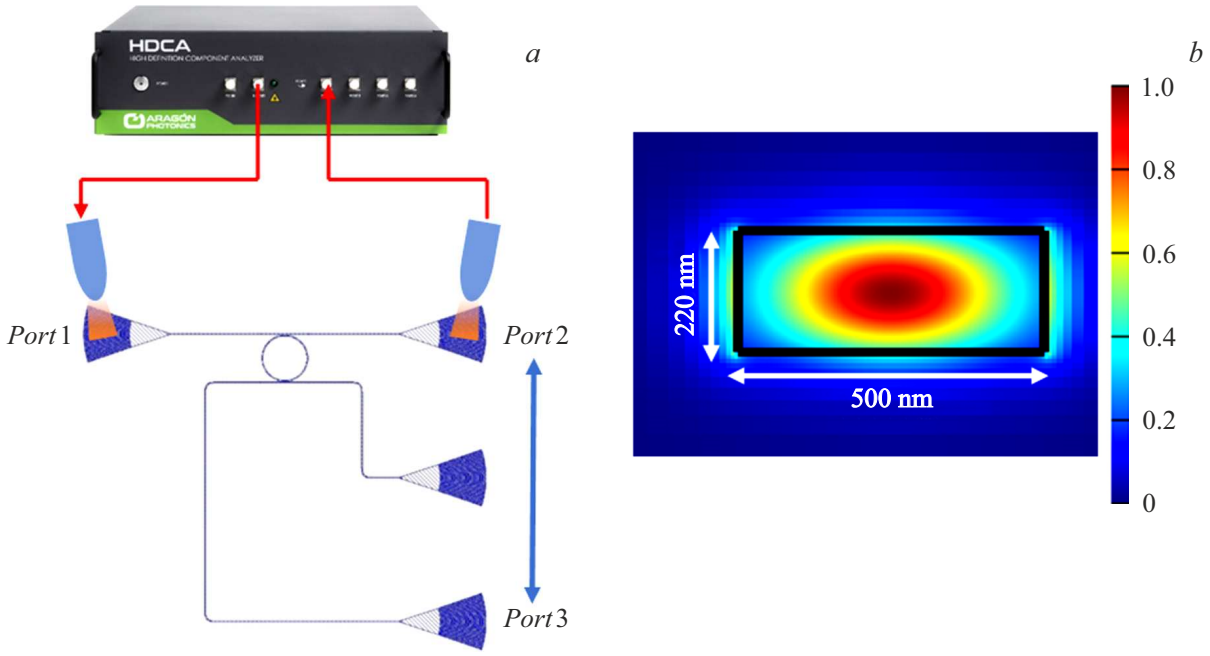

Figure 1. Setup for measurement of the transmission coefficient of an experimental SOI MRR prototype (a). Cross-section of the studied waveguide and the TE mode profile in it (b).

as dashed lines. It can be seen that the free spectral range at frequency 193 THz for a MRR with $d = 20\,\mu$m is $\Delta f = 1.14$ THz (Fig. 2, a, b). The increase of the ring diameter results in a decrease of the free spectral range to $\Delta f = 228$ GHz for $d = 100\,\mu$m (Fig. 2, c, d), to $\Delta f = 91$ GHz for $d = 256\,\mu$m (Figure 2, e,f). The insets to the figure show the transfer characteristics at a larger scale.

2. Model for determining the waveguide properties of integrated optical microwaveguides based on experimental transfer characteristics of MRR

Now let's proceed to the description of the model, which allows determining the waveguide properties of the optical MRR from the measured transfer characteristics. Consider a ring resonator consisting of a looped microwaveguide with a length of l and two straight waveguides used for input and output of an optical signal (Fig. 3). A part of the optical signal is coupled into the neighboring waveguide in the region where the distance between the input waveguide and the micro-ring resonator becomes small enough. This value is described by the coupling coefficient κ. Considering the losses in the coupling region to be negligible, we find that a single signal circulation in the ring symmetrically coupled with two input waveguides results in the decrease of the signal amplitude by $\kappa \cdot \exp(-\alpha l)$ times, where α is attenuation coefficient. In this case, the signal acquires an additional phase shift equal to βl. Then every single signal circulation in the ring shown in Figure 3 is described by the wave multiplier $\kappa \cdot \exp(-\alpha l) \cdot \exp(i\beta l)$. Let us denote the MRR coefficients of transmission from the input *1* (*port 1* in Fig. 1, a and 3) to the output *2* (*port 2* in Fig. 1, a and 3) and output *3* (*port 3* in Fig. 1, a and 3) as H_{p21} and H_{p31} respectively. H_{p21} and H_{p31} can be found using the partial wave method as the result of a superposition of circulating waves at the outputs *2* and *3* [6,47]:

$$H_{p21} = \frac{T_{21}t(1 - 2\mathrm{e}^{-\alpha l}\cos(\beta l) + \mathrm{e}^{-2\alpha l})}{1 - 2t\mathrm{e}^{-\alpha l}\cos(\beta l) + t^2\mathrm{e}^{-2\alpha l}}, \quad (1)$$

$$H_{p31} = \frac{T_{31}\mathrm{e}^{-\alpha l}\kappa^2}{1 - 2t\mathrm{e}^{-\alpha l}\cos(\beta l) + t^2\mathrm{e}^{-2\alpha l}}, \quad (2)$$

where the coefficient t means the fraction of power that remains in the waveguide after passing through the coupling region and is calculated as $t = 1 - \kappa$. T_{21} and T_{31} in expressions (1) and (2) describe the spectral efficiency of the lensed fibers and grating couplers for the signal input (through *port 1*) and output (through *port 2* and *3*). It should be noted that the lensed fiber positions are adjusted relative the grating couplers. Therefore, the coefficients T_{21} and T_{31} depend not only on the waveguide properties, but also on the optical fiber positioning accuracy, and, consequently, the input / output efficiencies are not equal to each other, i.e. $T_{21} \neq T_{31}$.

Fig. 4 qualitatively shows the transfer characteristics obtained from expressions (1) and (2). As can be seen, the characteristics demonstrate a multi-resonant response due to the in-phase interference of waves circulating in the ring.

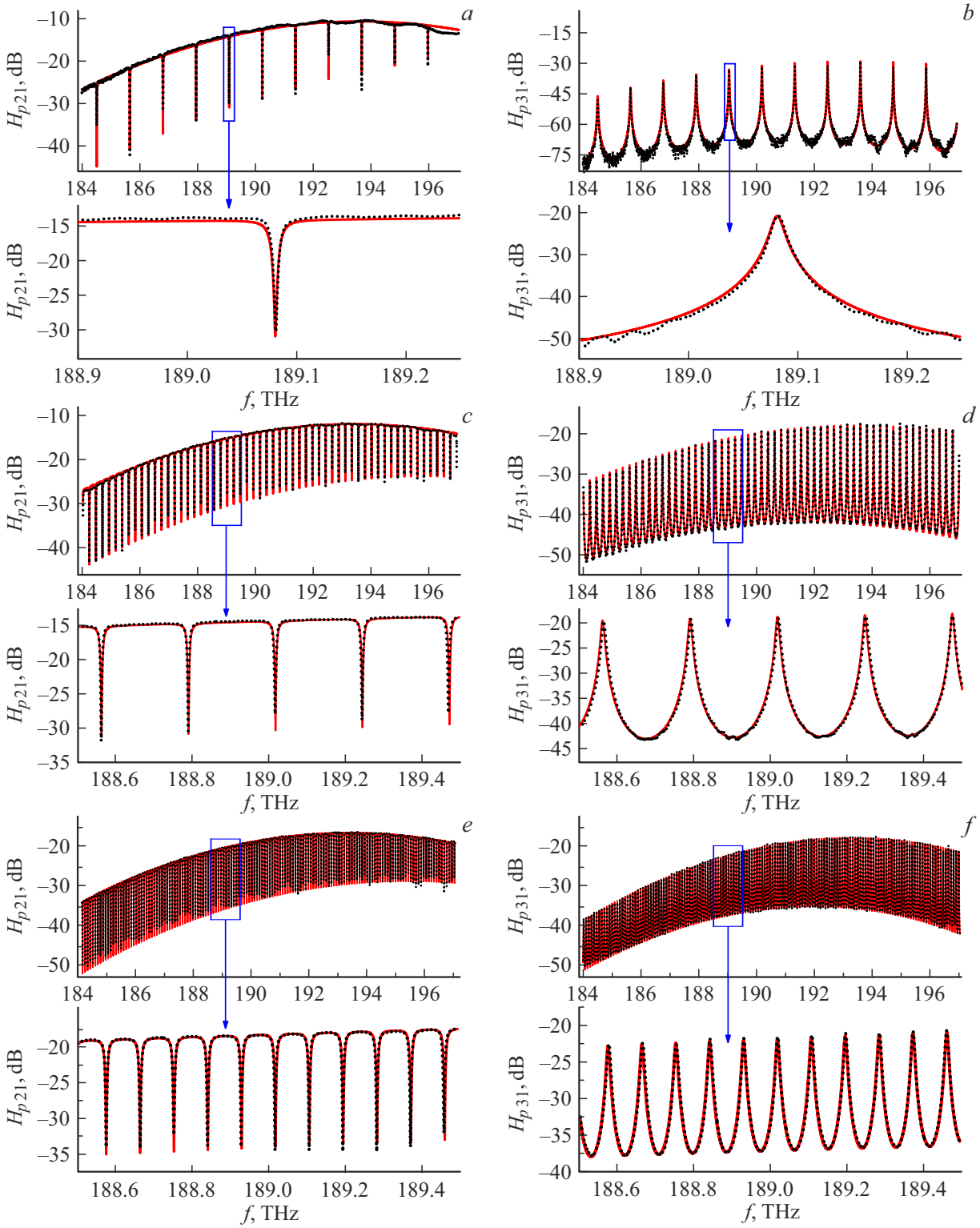

Figure 2. Experimental (points) and theoretical (lines) — transfer characteristics of MRR with diameters of $d = 20, 100, 256\,\mu$m. Tabs (*a*, *c*, *e*) show characteristics from the output *2*. Tabs (*b*, *d*, *f*) show characteristics from the output *3*.

Let's write down the resonant condition as

$$\beta_m = 2\pi m/l, \tag{3}$$

where m is the number of resonant harmonics.

Let's take a closer look at the transmission coefficient H_{21} (Fig. 4, *a*). It follows from the expressions (1) and (3) that $\cos(\beta_m l) = 1$ in the resonance. Then the transmission coefficient is minimal at the frequency corresponding to this

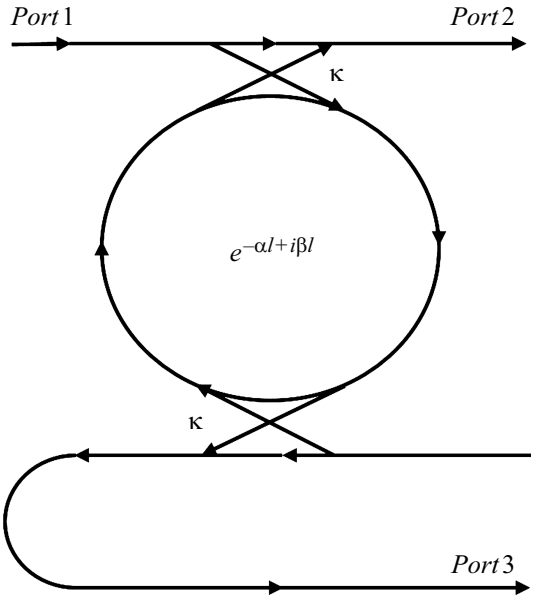

Figure 3. MRR circuit with two input waveguides.

wave number. The minimum value of the transmission coefficient $H_{p21\,\min}$ is shown by an asterisk in Figure 4, *a*. This value is determined using the formula:

$$H_{p21\,\min} = \frac{T_{21}t(1-\mathrm{e}^{-\alpha l})^2}{(1-t\mathrm{e}^{-\alpha l})^2}. \tag{4}$$

It is clear that the transmission coefficient H_{p21} has a maximum when $\beta = \pi(2m+1)/l$. The expression for the maximum transmission coefficient is obtained by substituting $\cos(\beta l) = -1$ in the expression (1) ($H_{p21\,\max}$ shown by an asterisk in Fig. 4, *a*):

$$H_{p21\,\max} = \frac{T_{21}t(1+\mathrm{e}^{-\alpha l})^2}{(1+t\mathrm{e}^{-\alpha l})^2}. \tag{5}$$

Let us similarly write down the expressions for the minimum (at $\beta = \pi(2m+1)/l$) and maximum (at $\beta_m = 2\pi m/l$) of the transmission coefficient H_{p31} ($H_{p31\,\min}$ and $H_{p31\,\max}$ are shown by asterisks in Fig. 4, *b*):

$$H_{p31\,\min} = \frac{T_{31}\mathrm{e}^{-\alpha l}\kappa^2}{(1+t\mathrm{e}^{-\alpha l})^2}, \tag{6}$$

$$H_{p31\,\max} = \frac{T_{31}\mathrm{e}^{-\alpha l}\kappa^2}{(1-t\mathrm{e}^{-\alpha l})^2}. \tag{7}$$

Next, let us divide the expressions (5) to (4) and (7) by (6), respectively. The following system of algebraic equations is obtained as a result:

$$\begin{cases} \dfrac{H_{p21\,\max}}{H_{p21\,\min}} = \dfrac{(1+\mathrm{e}^{\alpha l})^2(1-\kappa-\mathrm{e}^{\alpha l})^2}{(1-\kappa+\kappa\mathrm{e}^{\alpha l}-\mathrm{e}^{2\alpha l})^2}, & (a) \\ \dfrac{H_{p31\,\max}}{H_{p31\,\min}} = \dfrac{(1-\kappa+\mathrm{e}^{\alpha l})^2}{(1-\kappa-\mathrm{e}^{\alpha l})^2}. & (b) \end{cases} \tag{8}$$

Assume that the parameters α and κ slightly vary in the frequency range corresponding to the frequency distance between resonances. A system of equations for unknown parameters $\alpha(f_0)$ and $\kappa(f_0)$ is obtained by substituting the experimental values of maxima and minima of transmission coefficients H_{p21} and H_{p31} in the vicinity of the selected resonant frequency f_0 in the left side of the system of equations (8). The calculation is repeated for each resonant harmonic for determining the frequency dependences $\alpha(f)$, $\kappa(f)$.

Let's proceed to determining the dispersion properties of optical waveguides. MRR is a convenient tool for solving this problem, since the position of the resonant frequencies f_m is unambiguously related to the values of the resonant wave numbers β_m through the law of dispersion $\omega(\beta)$ of waves in the waveguide from which the MRR is made. First, let us expand $\omega(\beta)$ into a Taylor series in the vicinity of the frequency ω_0 and write this expansion in the following form:

$$\omega(\beta) = \omega_0 + \frac{c}{n_g}(\beta-\beta_0) + \frac{1}{2}D(\beta-\beta_0)^2, \tag{9}$$

where $\omega_0 = 2\pi f_0$, c is the speed of light, n_g is a group refractive index, D is the dispersion coefficient. The group refractive index n_g and the dispersion coefficient D are defined as follows in expression (9)

$$n_g = c\left(\frac{\partial\omega}{\partial\beta}\right)^{-1}, \tag{10}$$

$$D = \frac{\partial^2\omega}{\partial\beta^2}. \tag{11}$$

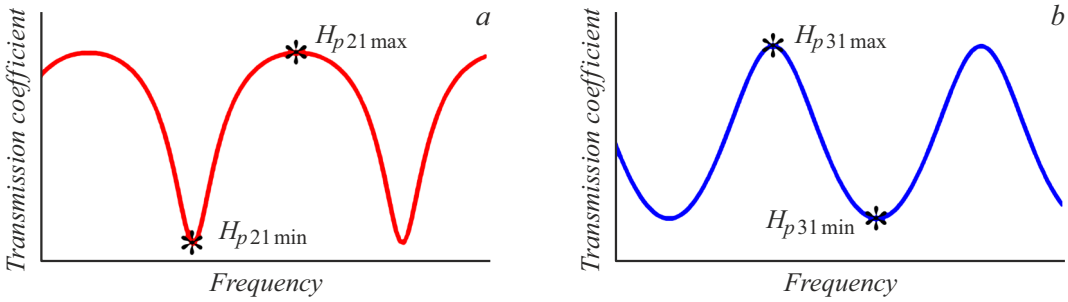

Figure 4. The MRR transmission coefficients H_{p21} (*a*) and H_{p31} (b).

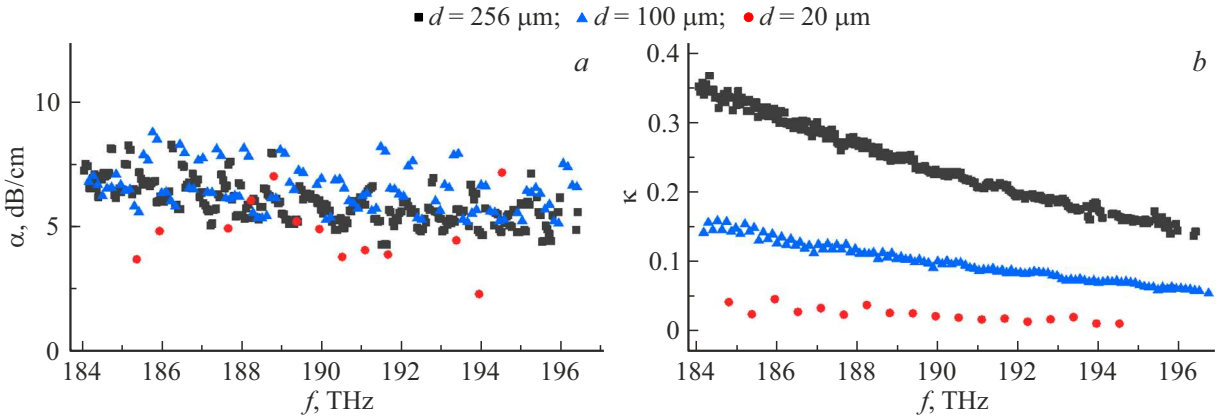

Figure 5. Dependence on the frequency of the attenuation α (a) and coupling coefficients κ (b) for rings with a diameter of $d = 256$ (black squares), 100 (blue triangles), 20 μm (red circles).

As can be seen from expressions (10) and (11), the frequency dependences of the parameters n_g and D can be obtained from experimental frequency dependences of the distance between resonances Δf, as well as the distance between neighboring resonant wave numbers $\Delta\beta$, which is determined solely by the ring length: $\Delta\beta = 2\pi/l$. After determining the above parameters, we define the coefficients T_{21} and T_{31} by comparing the theoretical transfer characteristics described by the expressions (1) and (2), with experimental data.

3. Experimental determination of the waveguide properties of integrated optical microwaveguides

We will use the proposed method to describe the waveguide properties of integrated optical SOI microwaveguides for verifying its adequacy. Fig. 5 shows the obtained frequency dependences. The scattering on the wall roughnesses is known as the main attenuation mechanism in the studied silicon waveguides [32,33,48,49], while the contribution of bending losses for resonators with a diameter greater than 10 μm is negligible [4,5], so the frequency dependences of the attenuation coefficients shown in Fig. 5, a demonstrates similar dependences. It should be noted that the propagation loss weakly decreases with the increase of the frequency from 7 dB/cm at a frequency of 185 THz to 5 dB/cm at a frequency of 197 THz. This behavior is associated with a decrease of the influence of waveguide wall roughness on the wave process [4]. The coupling coefficient also shows a decrease with the increase of the frequency as shown in Figure 5, b. In this case, a decrease of the ring diameter results in a reduction of the coupling region and a decrease of the coupling coefficient. It should be noted that this behavior is observed as long as a change of the bending radius weakly affects the field distribution in a curved waveguide.

One of the reasons for the deviation in determining the attenuation and coupling coefficients is the distortion present in the experimental transfer characteristics of the ring resonator. An attenuator was used in the experimental study of small-diameter ring, which resulted in an increase of noise and errors of determination of the attenuation and coupling coefficients in this case.

Let us use expressions (9) and (10) for determining the dispersion properties of waveguides by substituting in them the frequency dependences of the free spectral range $\Delta f(f)$ obtained from the experiment. The results of the calculation are shown in Fig. 6. It can be seen that all MRR have similar dispersion properties. Group refractive index is approximately $n_g = 4.179$ (Fig. 6, a), while the waveguides show a zero slope of the dispersion characteristic (Fig. 6, b). It should be noted that the error of determination of the group refractive index and dispersion coefficient is attributable to the accuracy of measuring the distance between the resonant frequencies. The convergence of resonant frequencies with increasing ring diameter results in an increase of the error for a given accuracy.

Let us remind that grating couplers were used for fiber-to-chip coupling. It is known that in the frequency range near the maximum the spectral efficiency of the such couplers has the Gaussian form [50]:

$$T = T_0 \cdot \exp\left(-\left(\frac{f - f_0}{\Delta}\right)^2\right), \qquad (12)$$

where T_0 is the maximum of the power transmission coefficient, f_0 is the frequency position of the maximum, Δ is the parameter that characterizes the width of the transmission characteristic. The obtained frequency dependences $\alpha(f)$, $n_g(f)$ and $\kappa(f)$ were used to calculate the theoretical values of the transfer characteristics according to expressions (1) and (2). The parameters included in the expression (12) were determined based on the best match of theory and experiment. The obtained values describing the frequency dependences of the coefficients T_{21} and T_{31} are presented

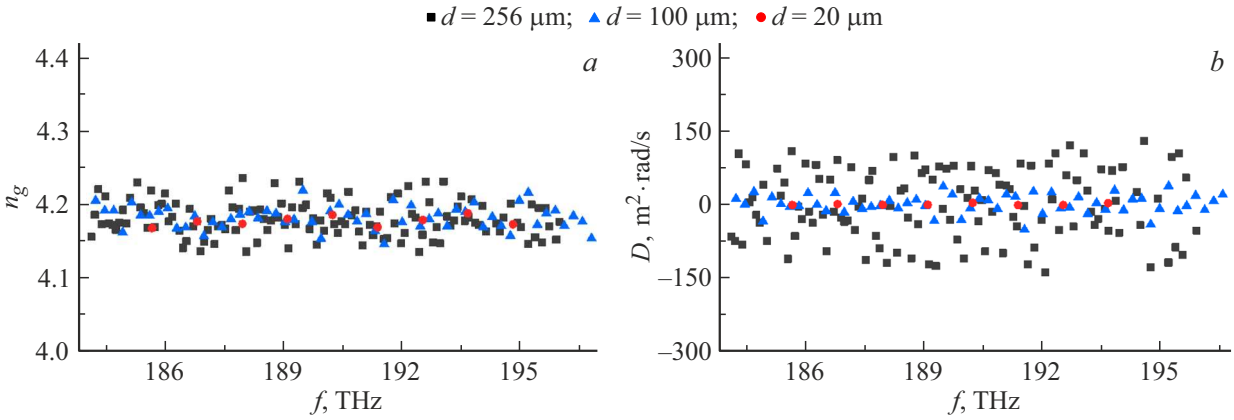

Figure 6. Dependence of the group refractive index n_g (a) and the dispersion coefficient D (b) on the frequency for rings with a diameter of $d = 256$ (black squares), 100 (blue triangles), 20 μm (red circles).

Input/output efficiency parameters

Parameter	MRR diameter(d), μm					
	256		100		20	
	T_{21}	T_{31}	T_{21}	T_{31}	T_{21}	T_{31}
T_0, dB	−14.7	−14.8	−11.3	−13.5	−10.7	−14.5
f_0, THz	193.28	193.7	193.4	194	193.6	194
Δ, THz	4.7	4.3	5	5.2	5	4.6

in the table. Small differences between T_{21} and T_{31} are attributable to errors of the manual alignment of the lensed fibers.

As a result, all the main parameters of the SOI microwaveguides were obtained in this paper. The theoretical and experimental characteristics of the MRR were compared to verify the adequacy of the proposed method. The transfer characteristics were numerically calculated according to expressions (1) and (2) using the obtained parameters. Theoretical characteristics are shown in Figure 2 by solid lines. It can be seen that the found frequency dependencies $\alpha(f)$, $n_g(f)$, $\kappa(f)$, $T_{21}(f)$ and $T_{31}(f)$ allow describing the transmission characteristics of the MRR with high accuracy, which confirms the adequacy of the developed method.

Conclusion

The waveguide properties of integrated optical microwaveguides and MRR based on them were experimentally determined in a wide frequency range. An analytical method for extraction the frequency dependences of the attenuation and coupling coefficients, the group refractive index, the dispersion coefficient, as well as the spectral efficiency of fiber-to-chip coupling from on the measured transfer characteristics of MRR was developed. The dependences of the listed parameters of silicon MRR of various diameters in the frequency range from 184 to 197 THz were obtained in the paper. It was shown that the attenuation coefficient in experimental samples of silicon waveguides does not depend on the resonator radius and weakly decreases with the increase of the frequency: from 7 dB/cm at a frequency of 185 THz to 5 dB/cm at a frequency of 197 THz. The coupling coefficient increases with the resonator diameter. It demonstrates an inversely proportional dependence on frequency in this case. The silicon waveguides showed weak dispersion properties in the frequency range under investigation. The group refractive index was about 4.179. It should be noted that the obtained value differs from the theoretical one, which is 4.203 at a frequency of 191.5 THz for silicon waveguides with the cross section of 500 × 220 nm. Such a difference may be attributable to the difference between the actual dimensions of the waveguide and the designed dimensions as shown in studies [31,40]. The frequency dependences describing the efficiency of fiber-to-chip coupling were obtained by combining experimental and theoretical characteristics at the final stage. The found parameters are used for modeling the transfer characteristics of ring resonators. A conclusion about the applicability of the proposed method is made through the comparison of experimental and theoretical results. It should be noted that one ring resonator with a diameter of 20 μm is sufficient to study the waveguide parameters. Such a small size of the test elements allows for their even positioning on the surface of the studied chip, which can be used for local determination of PIC parameters and construction of spatial distributions of waveguide parameters. In addition, the proposed method can be extended by adding an equation for the width of the resonant curve [44] or by including the resonator in the arm of the Mach-Zehnder interferometer [45,46], which allows increasing the number of determined waveguide parameters, for example, coupling

coefficients in an unbalanced coupled ring resonator or attenuation in the coupling region.

Funding

This study was supported by the Ministry of Science and Higher Education of the Russian Federation (grant № FSEE-2022-0017).

Conflict of interest

The authors declare that they have no conflict of interest.

References

[1] D. Marpaung, J. Yao, J. Capmany. Nature Photonics, **13** (2), 80 (2019). DOI: 10.1038/s41566-018-0310-5
[2] D. Zhu, L. Shao, M. Yu, R. Cheng, B. Desiatov, C.J. Xin, Y. Hu, J. Holzgrafe, S. Ghosh, A. Shams-Ansari, E. Puma, N. Sinclair, C. Reimer, M. Zhang, M. Lončar. Adv. Opt. Photon., **13** (2), 242 (2021). DOI: 10.1364/AOP.411024
[3] S. Shekhar, W. Bogaerts, L. Chrostowski, J.E. Bowers, M. Hochberg, R. Soref, B.J. Shastri. Nature Commun., **15** (1), 751 (2024). DOI: 10.1038/s41467-024-44750-0
[4] Y.A. Vlasov, S.J. McNab. Opt. Express, **12** (8), 1622 (2004). DOI: 10.1364/OPEX.12.001622
[5] W. Bogaerts, S.K. Selvaraja. IEEE Photon. J., **3** (3), 422 (2011). DOI: 10.1109/JPHOT.2011.2142931
[6] W. Bogaerts, P. De Heyn, T. Van Vaerenbergh, K. De Vos, S. Kumar Selvaraja, T. Claes, P. Dumon, P. Bienstman, D. Van Thourhout, R. Baets. Laser Photon. Rev., **6** (1), 47 (2012). DOI: 10.1002/lpor.201100017
[7] L. Vivien, L. Pavesi. *Handbook of Silicon Photonics* (Taylor & Francis, 2016), DOI: 10.1201/b14668
[8] W. Bogaerts, L. Chrostowski. Laser Photon. Rev., **12** (4), 1700237 (2018). DOI: 10.1002/lpor.201700237
[9] S.Y. Siew, B. Li, F. Gao, H.Y. Zheng, W. Zhang, P. Guo, S.W. Xie, A. Song, B. Dong, L.W. Luo, C. Li, X. Luo, G.-Q. Lo. J. Lightwave Technol., **39** (13), 4374 (2021). DOI: 10.1109/jlt.2021.3066203
[10] W. Bogaerts, S.K. Selvaraja, P. Dumon, J. Brouckaert, K. De Vos, D. Van Thourhout, R. Baets. IEEE J. Selected Topics in Quant. Electron., **16** (1), 33 (2010). DOI: 10.1109/JSTQE.2009.2039680
[11] W. Bogaerts, S. Pathak, A. Ruocco, S. Dwivedi. Integrated Optics: Devices, Mater., Technol. XIX, **9365**, 42 (2015). DOI: 10.1117/12.2082785
[12] F. Horst, W.M. Green, S. Assefa, S.M. Shank, Y.A. Vlasov, B.J. Offrein. Opt. Express, **21** (10), 11652 (2013). DOI: 10.1364/OE.21.011652
[13] B. Zhang, K. Al Qubaisi, M. Cherchi, M. Harjanne, Y. Ehrlichman, A.N. Khilo, M.A. Popović. Opt. Lett., **45** (11), 3005 (2020). DOI: 10.1364/OL.395203
[14] K. Jia, W. Wang, Y. Tang, Y. Yang, J. Yang, X. Jiang, Y. Wu, M. Wang, Y. Wang. IEEE Photon. Technol. Lett., **17** (2), 378 (2005). DOI: 10.1109/LPT.2004.839394
[15] G.B. Cao, F. Gao, J. Jiang, F. Zhang. IEEE Photon. Technol. Lett., **17** (8), 1671 (2005). DOI: 10.1109/LPT.2005.851959
[16] G.T. Reed, G. Mashanovich, F.Y. Gardes, D. Thomson. Nature Photon., **4** (8), 518 (2010). DOI: 10.1038/nphoton.2010.179
[17] Q. Xu, S. Manipatruni, B. Schmidt, J. Shakya, M. Lipson. Opt. Express, **15** (2), 430 (2007). DOI: 10.1364/OE.15.000430
[18] L. Vivien, A. Polzer, D. Marris-Morini, J. Osmond, J.M. Hartmann, P. Crozat, E. Cassan, C. Kopp, H. Zimmermann, J.M. Fédéli. Opt. Express, **20** (2), 1096 (2012). DOI: 10.1364/OE.20.001096
[19] L. Chen, M. Lipson. Opt. Express, **17** (10), 7901 (2009). DOI: 10.1364/OE.17.007901
[20] R. Soref, B. Bennett. IEEE J. Quant. Electron., **23** (1), 123 (1987). DOI: 10.1109/JQE.1987.1073206
[21] R. Dekker, N. Usechak, M. Först, A. Driessen. J. Phys. D: Appl. Phys., **40** (14), R249 (2007). DOI: 10.1088/0022-3727/40/14/R01
[22] A.A. Nikitin, I.A. Ryabcev, A.A. Nikitin, A.V. Kondrashov, A.A. Semenov, D.A. Konkin, A.A. Kokolov, F.I. Sheyerman, L.I. Babak, A.B. Ustinov. Opt. Commun., **511**, 127929 (2022). DOI: 10.1016/j.optcom.2022.127929
[23] A.A. Nikitin, A.V. Kondrashov, V.V. Vitko, I.A. Ryabcev, G.A. Zaretskaya, N.A. Cheplagin, D.A. Konkin, A.A. Kokolov, L.I. Babak, A.B. Ustinov, B.A. Kalinikos. Opt. Commun., **480**, 126456 (2021). DOI: 10.1016/j.optcom.2020.126456
[24] S. Zhuang, J. Feng, H. Liu, S. Yuan, Y. Chen, H. Zeng. Opt. Commun., **507**, 127637 (2022). DOI: 10.1016/j.optcom.2021.127637
[25] M. Borghi, S. Biasi, L. Pavesi. Sci. Reports, **11** (1), 15642 (2021). DOI: 10.1038/s41598-021-94952-5
[26] H. Zhang, J. Wen, Z. Wu, Q. Wang, H. Yu, Y. Zhang, Y. Pan, L. Yin, C. Wang, S. Qu. Opt. Commun., **558**, 130374 (2024). DOI: 10.1016/j.optcom.2024.130374
[27] X. Ji, S. Roberts, M. Corato-Zanarella, M. Lipson. APL Photon., **6** (7), 071101 (2021). DOI: 10.1063/5.0057881
[28] J. Liu, G. Huang, R.N. Wang, J. He, A.S. Raja, T. Liu, N.J. Engelsen, T.J. Kippenberg. Nature Commun., **12** (1), 2236 (2021). DOI: 10.1038/s41467-021-21973-z
[29] W. Jin, Q.F. Yang, L. Chang, B. Shen, H. Wang, M.A. Leal, L. Wu, M. Gao, A. Feshali, M. Paniccia, K.J. Vahala, J.E. Bowers. Nature Photon., **15** (5), 346 (2021). DOI: 10.1038/s41566-021-00761-7
[30] W.D. Sacher, J.C. Mikkelsen, Y. Huang, J.C.C. Mak, Z. Yong, X. Luo, Y. Li, P. Dumais, J. Jiang, D. Goodwill, E. Bernier, P.G.-Q. Lo, J.K.S. Poon. Proceed. IEEE, **106** (12), 2232 (2018). DOI: 10.1109/JPROC.2018.2860994
[31] Y. Xing, J. Dong, S. Dwivedi, U. Khan, W. Bogaerts. Photon. Res., **6** (11), 1008 (2018). DOI: 10.1364/PRJ.6.001008
[32] K.K. Lee, D.R. Lim, H.C. Luan, A. Agarwal, J. Foresi, L.C. Kimerling. Appl. Phys. Lett., **77** (11), 1617 (2000). DOI: 10.1063/1.1308532
[33] K.K. Lee, D.R. Lim, L.C. Kimerling, J. Shin, F. Cerrina. Opt. Lett., **26** (23), 1888 (2001). DOI: 10.1364/OL.26.001888
[34] D.G. Rabus. *Integrated Ring Resonators* (Springer-Verlag Berlin Heidelberg, 2007)
[35] I.P. Kaminow, L.W. Stulz. Appl. Phys. Lett., **33** (1), 62 (1978). DOI: 10.1063/1.90191
[36] T. Feuchter, C. Thirstrup. IEEE Photon. Technol. Lett., **6** (10), 1244 (1994). DOI: 10.1109/68.329652
[37] A.S.A. Sakai, G.H.G. Hara, T.B.T. Baba. Jpn. J. Appl. Phys., **40** (4B), L383 (2001). DOI: 10.1143/JJAP.40.L383
[38] V.R. Almeida, R.R. Panepucci, M. Lipson. Opt. Lett., **28** (15), 1302 (2003). DOI: 10.1364/OL.28.001302
[39] C.J. Oton, C. Manganelli, F. Bontempi, M. Fournier, D. Fowler, C. Kopp. Opt. Express, **24** (6), 6265 (2016). DOI: 10.1364/OE.24.006265

[40] A.A. Ershov, A.I. Eremeev, A.A. Nikitin, A.B. Ustinov. Microwave Opt. Technol. Lett., **65** (8), 2451 (2023). DOI: 10.1002/mop.33675
[41] Y. Gottesman, E.V.K. Rao, D.G. Rabus. J. Lightwave Technol., **22** (6), 1566 (2004). DOI: 10.1109/JLT.2004.829216
[42] Y. Gottesman, D.G. Rabus, E.V.K. Rao, B.-E. Benkelfat. IEEE Photon. Technol. Lett., **21** (19), 1399 (2009). DOI: 10.1109/LPT.2009.2025603
[43] I. A. Ryabcev, A. A. Ershov, D. V. Ryaikkenen, A. P. Burovikhin, R. V. Haponchyk, I. Yu. Tatsenko, A. A. Stashkevich, A. A. Nikitin, A. B. Ustinov. Journal of the Russian Universities. Radioelectronics, **25** (6), 79 (2022) (in Russian). DOI: 10.32603/1993-8985-2022-25-6-79-89
[44] W.R. McKinnon, D.-X. Xu, C. Storey, E. Post, A. Densmore, A. Delâge, P. Waldron, J.H. Schmid, S. Janz. Opt. Express, **17** (21), 18971 (2009). DOI: 10.1364/OE.17.018971
[45] J.E. Heebner, V. Wong, A. Schweinsberg, R.W. Boyd, D.J. Jackson. IEEE J. Quant. Electron., **40** (6), 726 (2004). DOI: 10.1109/JQE.2004.828232
[46] F. Xia, L. Sekaric, Y.A. Vlasov. Opt. Express, **14** (9), 3872, (2006). DOI: 10.1364/OE.14.003872
[47] A.A. Nikitin, V.V. Vitko, M.A. Cherkasskii, A.B. Ustinov, B.A. Kalinikos. Results Phys., **18**, 103279 (2020). DOI: 10.1016/j.rinp.2020.103279
[48] F. Grillot, L. Vivien, S. Laval, E. Cassan. J. Lightwave Technol., **24** (2), 891 (2006). DOI: 10.1109/JLT.2005.861939
[49] L. Chrostowski, M. Hochberg. *Silicon Photonics Design: from Devices to Systems* (Cambridge University Press, 2015)
[50] D. Taillaert, P. Bienstman, R. Baets. Opt. Lett., **29** (13), 2749 (2004). DOI: 10.1364/OL.29.002749

Translated by A.Akhtyamov

Translated by A.Akhtyamov